

# REYNOLDS NUMBER EFFECTS IDENTIFIED WITH CFD METHODS COMPARED TO SEMI-EMPIRICAL METHODS

**Karl Pettersson, Arthur Rizzi**  
**Department of Aeronautical and Vehicle Engineering, AVE**  
**Royal Institute of Technology (KTH)**  
**Teknikringen 8**  
**SE-100 44 Stockholm, Sweden**

**Keywords:** *aeronautics, CFD, Reynolds number, scaling, corrections*

## Abstract

*In order to estimate Reynolds number effects on a transonic transport aircraft CFD calculations have been performed. The CFD calculations have been done solving the RANS equations on an unstructured grid for varying Reynolds number at transonic conditions. Low Reynolds number data have been extrapolated to a higher Reynolds number condition with different scaling methodologies in order to evaluate each methods strengths and weaknesses.*

## 1 Introduction

According to Covert [4], a L/D estimation of  $\pm 5\%$  is to be rated as a “very good” result when comparing data from the detailed design phase with the actual flight test data. Conservatism or a badly predicted L/D at the design stage will result in an inefficient engine and a noncompetitive airplane or a costly step backwards to a previous design stage in order to correct the erroneous estimates. According to Barlow [1], time is seldom available to back up and correlate free flight data with wind tunnel data. If this is done the results are generally considered company proprietary because of the high cost associated with obtaining them. Some of the differences between

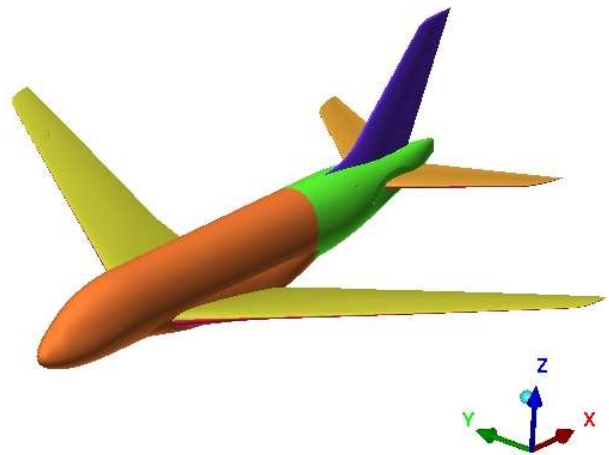


**Fig. 1** The transonic transport aircraft investigated.

wind tunnel estimates and free flight performance are due to scale effects. Some of these scale effects might be due to differences in Reynolds number between the wind tunnel and the free flight condition. This work has been done within the REMFI consortium [7]. One of the objectives in this project has been to evaluate the Reynolds number scaling effects and to do so CFD calculations have been performed. When comparing wind tunnel results with CFD or free flight results some scaling effects could be anticipated. Some of these effects are; having various gaps in the wind tunnel model which are not present in the CFD model, wall blockage effects and wind tunnel mounting effects, also called geometrical differences. Changing Reynolds num-

---

Copyright © 2006 by Karl Pettersson. Published by the International Council of the Aeronautical Sciences with permission. Paper number: ICAS 2006-2.3.4

ber by increasing pressure might influence the aeroelastic effects of the wind tunnel model. The wind tunnel model might have a different stiffness from the free flight aircraft and it differs for sure when comparing it to the infinitely stiff CFD model. Wind tunnel turbulence might also change with varying Reynolds number and effects like these which initially may appear to be due to changes in Reynolds number might actually depend on some other wind tunnel variable changing as well. There might actually be one or more variables that might change with varying Reynolds number and these effects, called pseudo-Reynolds effects as cited in Haines [8], could easily be interpreted as Reynolds number effects. Artificial dissipation or turbulence modeling could be categorized as a pseudo-Reynolds number effect when dealing with CFD. Before conclusions can be drawn about the turbulence model used or the results obtained one has to assure that the influence of mesh- and residual dependence and round off and truncation errors have been minimized. Some of the wind tunnel pseudo-Reynolds number effects, like those associated with wall interference and tunnel calibration, which may vary in a non-linear way with Reynolds number, could however easily be excluded in the CFD calculations and an investigation of the true Reynolds number effects minimizing pseudo-Reynolds number effects could be done.

Reynolds number effects in large can be divided into direct and indirect effects. The direct effects are the ones that occur when the pressure distribution is frozen for varying Reynolds number e.g. skin friction on a flat plate with zero pressure gradient. The indirect effects are Reynolds number effects that involves a change in pressure distribution for varying Reynolds number. The order of magnitude of the indirect Reynolds number effects might have an impact on the feasibility of scaling methods which incorporates skin-friction estimates based on flat plate flow to account for Reynolds number variation.

One could always argue whether or not to trust absolute numbers from CFD calculations when having results such as the second AIAA

drag prediction workshop data in mind, see Hensch [10] amongst others. The results in  $C_D$  between partners could differ with as much as 40 drag counts (where one count is 1/10000) for calculations with the same mesh but with different solvers and turbulence models. The outlook compared to the first drag prediction workshop however is brighter. The scatter in computed  $C_D$  for partners in the second workshop has been decreased with almost a factor of three compared to the first workshop and the mean of the CFD results differed with approximately three drag counts compared to wind tunnel data. Scaling methodology has according to Bushnell [2] improved compared to earlier experience due to the increased use of CFD and the availability of new high Reynolds number transonic facilities. This work tries to make use of the increased accuracy in CFD methods in order to estimate and isolate true Reynolds number effects on a transonic transport aircraft.

## 2 CFD calculations

The following sections describes the CFD code, mesh generation and CFD calculations. The first part describes the CFD code and turbulence modeling used. The second part describes how a mesh can be produced with different programs using the best features of each program in order to produce a high quality mesh and the last part describes mesh and residual dependence. In order to evaluate Reynolds number scaling effects three different Reynolds numbers (20, 38 and 56 million) have been evaluated. The free stream Mach number has been held constant at 0.85 at an angle of attack of  $0^\circ$ .

### 2.1 Description of the CFD code

The CFD calculations have been done using the latest development version of Edge [6], v.3.3.2-r506. Edge is an unstructured, edge-based, finite volume code developed by the Swedish Defence Research Agency (FOI). When the time independent problem is solved, a local time stepping approach is used with an explicit three-stage

Runge-Kutta scheme. The spatial discretization utilizes a second order central difference scheme with artificial dissipation. The turbulent quantities are discretized with a second order up-wind scheme. In order to speed up convergence four multigrid levels with implicit residual smoothing have been used.

Turbulence has been modeled with a  $k-\omega$  model, developed by Hellsten [9], coupled with an explicit algebraic Reynolds stress model; W&J EARSM created by Wallin and Johansson [18]. It is possible to assign regions with laminar flow in `Edge` but these calculations have been done using a fully turbulent flow. The laminar regions of the flow on the aircraft are assumed to be small at these Reynolds numbers (20, 38 and 56 million) and the assumption of fully turbulent flow were judged to be reasonable. The far-field boundary condition for turbulence intensity was set to 0.1%.

## 2.2 Mesh generation

Generating a mesh can be tedious and time consuming work when the underlying CAD geometry is corrupt. The most unstructured mesh programs will have problems with bad CAD geometries, such as overlapping patches and holes. A structured mesher has the advantage of additional user defined information such as curve to edge and surface to face association (where curves and surfaces belongs to the CAD topology and edges and faces to the mesh topology). This extra information usually makes the mesher more capable of running over bad CAD parts. One way to use the structured meshing technique with the advantage of being more capable of handling bad CAD geometries and creating a high quality unstructured mesh in the end is given as a guide below. Since the problem at hand is symmetric (the side-slip angle of the wind is zero) the obvious start when meshing is to neglect one side of the geometry and use a symmetric boundary condition. The following procedure was used in order to generate the surface and volume mesh. The unstructured surface mesh was first generated using the commercial mesher ICEM CFD

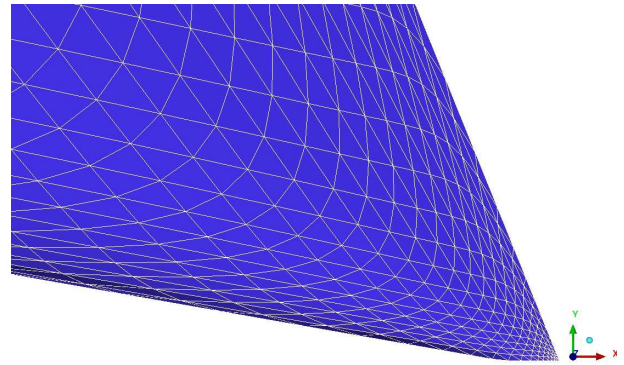


**Fig. 2** Isotropic and anisotropic mesh at the tip of the htp.

with the “patch independent” triangle mesher for the fuselage, wing and vertical tail plane (vtp). The horizontal tail plane (htp) was meshed with a structured surface mesh in order to get quads with the appropriate spacing and stretching in flow dependent directions. This surface mesh was converted into triangles and merged together with the rest of the mesh using the program `tgrid`, which is part of the commercial program suite of Fluent. The htp, with its delicate features (a very thin trailing edge), then consisted of a high quality mesh with an isotropic mesh where the wall curvature is low and an anisotropic mesh where the wall curvature is high and where the mesh is close to the trailing edge, see figure 2. A volume mesh, which consisted of tetrahedra only, was generated in ICEM CFD using the surface mesh and density functions as the only input to the mesher. The volume mesh was exported to TRITET (see Tysell [16]). TRITET used the volume mesh from ICEM as a “background” grid, a starting point in the advancing front technique, in order to generate a high quality hybrid RANS mesh. For the Reynolds number 38 million case, a first cell height of  $2 \times 10^{-5}$  meters was chosen. The nodes in the wall normal direction were distributed with an exponential growth function. A total prism height of 0.3 meters was assigned in order to capture the thick boundary layer at the rear end of the fuselage. The use of 40 prism layers resulted in a ratio of spacing of 1.23. A cut of

the resulting volume mesh is shown in figure 3.

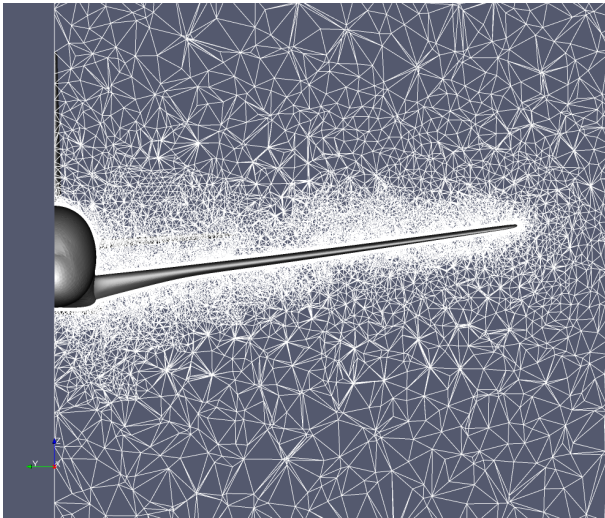


**Fig. 3** Cut of the volume mesh along the sweep of the wing.

### 2.3 Residual and mesh dependence

To assure a grid and residual independent solution the Reynolds number 20 million case was first computed and investigated. The baseline mesh consisted of 3.4 million tetrahedra and 15.9 million pentas. For the baseline mesh the change in  $C_D$  is less than one drag count when comparing the results for -5.5 and -6.5 for scaled density residual. The converged base line mesh was then adapted (h-adapted, i.e. dividing cells) with respect to density, velocity and pressure gradients which resulted in a mesh consisting of 4.7 million tetrahedra and 16.6 million pentas. A change in  $C_D$  which was less than one drag count was observed when comparing the results for -5.5 and -6.5 for scaled density residual. The converged base line mesh and the converged adapted mesh differed with approximately three drag counts when comparing results with a scaled density residual of -6.5. A summary of the mesh and residual dependence is given in table 1 where the difference in drag are measured in drag counts and relative to the baseline mesh with a residual of -5.5.

Further refinements of the mesh was judged unnecessary. A multigrid approach was used

**Table 1** Mesh and residual dependence on  $C_D$  in drag counts relative to the baseline mesh with a residual of -5.5.

mesh	residual -5.5	residual -6.5
baseline	0	0
adapted	-3	-3

within the solver in order to speed up convergence. Figure 4 shows a typical convergence history. In this case four multigrid levels have been used with the adapted mesh at a Reynolds number of 20 millions. Each tick on the y axis in the force graph represent one drag count and the x axis starts and stops at positions corresponding to scaled density residuals of -5.5 and -6.5 respectively. The curve has flattened out for the last 200 iterations and there is a relatively small change in  $C_D$  at the end of the calculations. The relatively small change in  $C_D$  when comparing residuals of -5.5 and -6.5 concluded that the -6.5 residual convergence criteria would be enough to ensure a residual independent solution.

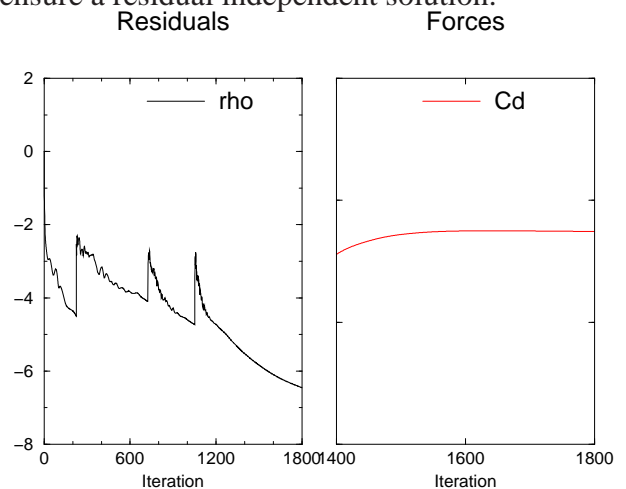


**Fig. 4** Convergence history for the adapted mesh at Reynolds number 20 million.

In order to resolve the boundary layer accurately a  $y^+$  less than four and at least five to ten mesh points between the wall and a  $y^+$  of 20 are required. [3] An inspection of  $y^+$  was done for all Reynolds number cases. The typical value of  $y^+$  was in the range of 0.5 and 2 for all wall bound-

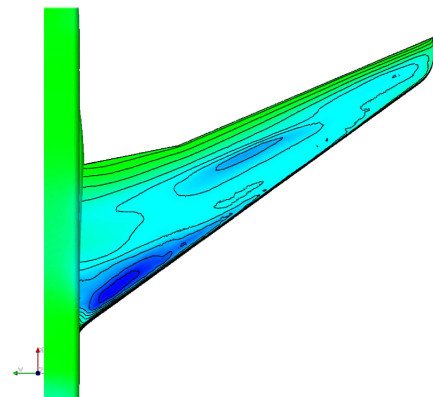
ary conditions and Reynolds numbers. There was typically seven mesh points for a  $y^+$  less than or equal to 20.

### 3 Results

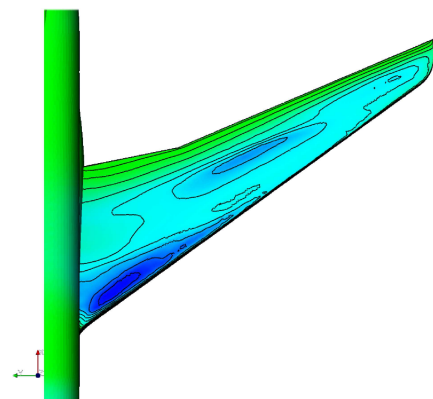
When the investigation of mesh and residual dependence and an inspection of  $y^+$  were done, the Reynolds number 20, 38 and 56 million cases were computed. The free stream Mach number was held constant at 0.85 with an angle of attack of  $0^\circ$ . The CFD results were then post-processed in the open-source visualization program ParaView.

The pressure distribution and skin friction was examined for the wing for varying Reynolds number. The pressure coefficient,  $c_p$ , is plotted in figure 5 together with iso-lines. The range of the color plot of  $c_p$  and the values for which the iso-lines are plotted are held constant for varying Reynolds number in order to make comparisons easier. No large change in pressure distribution is seen. There are some influences in the pressure distribution on the wing tip and leading edge area of the wing, but these effects are relatively small and are assumed to have a small influence on drag due to pressure.

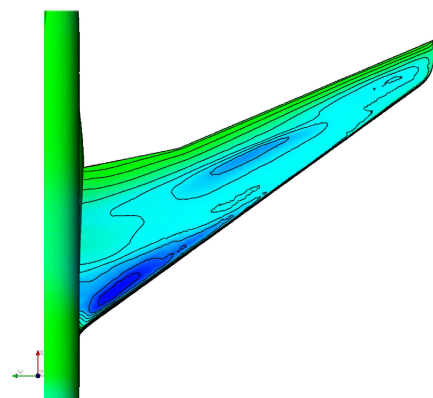
Variation in Reynolds number is however assumed to have an influence on skin friction. In order to estimate changes in the flow topology, the stream lines of skin friction has been visualized in figure 6. The surface has been plotted with the x component of skin friction and has an upper limit of zero in order to easily establish where reversed flow exists (flow which has a negative component of skin friction in x direction). The stream lines of skin friction over the wing has been visualized “seeding” the streams with the same points for all Reynolds number. This was done in order to ease the inspection of the flow topology and be able to compare the same set of stream lines for varying Reynolds number. A relatively small change in flow topology is seen over the Reynolds number range. It is also noted that the flow stays attached over the wing for varying Reynolds number. One region where the flow over the fuselage is detached is



(a) Iso-lines of  $c_p$  at Reynolds 20 million.



(b) Iso-lines of  $c_p$  at Reynolds 38 million.



(c) Iso-lines of  $c_p$  at Reynolds 56 million.

**Fig. 5** Wing seen from above, colored by  $c_p$  with iso-lines of  $c_p$ .

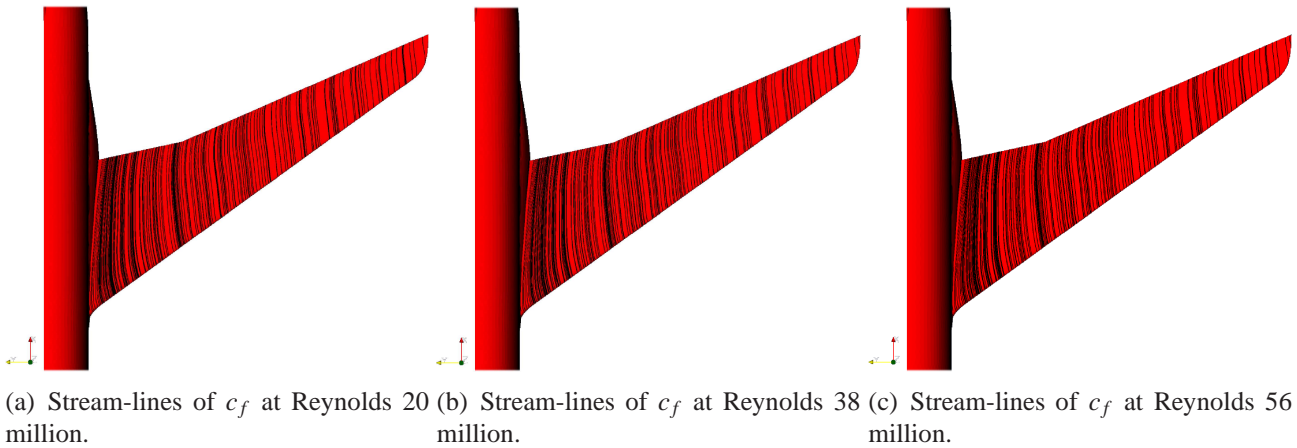


**Fig. 6** Wing seen from above, colored by  $c_f$  with stream-lines of  $c_f$ .

seen in figure 7. The x component of skin friction is visualized together with stream lines of skin friction. The color range of  $c_f$  varies between  $-10^{-6}$  and  $10^{-6}$ . This makes it easier to identify the region where the flow has a negative value of skin friction in the x direction. The flow is reversed in the front part of the fuselage/htp junction. The flow developed along the fuselage is heavily dependent on Reynolds number and the length of the separation bubble will hence probably be Reynolds number dependent. A visual

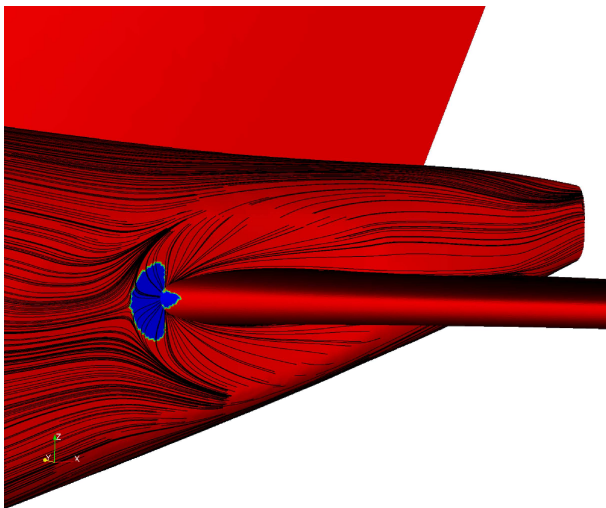


**Fig. 7** Separation of the flow at the htp/fuselage junction, at Reynolds number 20 million.

inspection of the length of the separation bubble were done for all Reynolds numbers. The length of the separation bubble decreased with approx-

imately 3% when comparing the 20 with the 38 million Reynolds number case. When comparing the 38 to the 56 million Reynolds number case the length of the separation bubble decreased once again with approximately 3%.

#### 4 Reynolds number scaling

Scaling methodology is not synonymous to Reynolds number effects only, but could also include effects of wind tunnel wall corrections for example as well. In this section, only Reynolds number effects will be addressed, in order to give an overview of a few Reynolds number scaling approaches. The Reynolds number effects identified with CFD methods will hopefully minimize the effects of pseudo-Reynolds number effects. This will enable comparisons between corrected wind tunnel data and CFD data in order to estimate free flight conditions.

The drag force in general consists of one normal component and one tangential to the surface. The tangential component is due to friction forces while the normal is due to pressure forces. The pressure force is dependent on parameters such as wall curvature and compressibility effects amongst others. This effect is hence dependent on geometry and temperature. Wall shear stress or friction will also be dependent on temperature, since viscosity varies with temperature, but it will also be dependent on whether the flow is laminar or turbulent. A need for estimating

the influence of transition position and changes in compressible effects is now obvious in order to scale drag for varying Reynolds number. The problem at hand is to predict the change in drag due to friction and pressure for varying Reynolds number in an accurate way, incorporating effects of topological changes and pressure variations in the flow. For a flat plate flow the change in  $C_F$  for varying Reynolds number is relatively smooth and the pressure gradient is unchanged and there is only direct Reynolds number effects present. This smooth effect and constant pressure distribution might no longer exist when the flow passes a curved surface, for example an airfoil. One example of the topological change of the flow for varying Reynolds number is given by Schewe [14]. When the Reynolds number is below a critical Reynolds number (sub-critical flow), the incompressible flow is relatively uniform over the two dimensional wing. When the Reynolds number is larger than the critical Reynolds (super-critical flow) number however, the flow changes and the oil flow now shows an “owl eyes” topology instead. The effects encountered here, changes in the appearance of the oil flow and transition position, are likely to have an impact on skin friction. Another example, including changes in the compressible effects, for varying Reynolds number is also given in order to illustrate some typical Reynolds number effects that could be encountered. The effect of a thinner boundary layer for a higher Reynolds number implies a higher effective camber of a wing and this might move potential shock waves in chord-wise direction. The change in position and strength of the shock wave might separate the flow and these effects combined, could have a large impact on the pressure distribution over the wing. These Reynolds number effects implies a significant change in pressure distribution and these effects are said to be; indirect Reynolds number effects. A classical example of this effect is the observation of movement of shock position comparing wind tunnel and free flight data for the Lockheed C-141 transport aircraft. This investigation, done in the 1960s, is an example of the drastic effects of pressure distribution change due

to a disproportionate boundary layer thickness. This lead to the establishment of a boundary layer scaling criterion for airfoils with different pressure distributions (as cited in [13]). Estimating Reynolds number scaling effects in a wind tunnel might be conducted using either a Reynolds number or a transition sweep. In the second case a simulation criterion has to be chosen in order to give the same viscous flow behavior in the wind tunnel with its forced transition at low Reynolds number as the free flight condition with its high Reynolds number and natural transition.

A suitable choice of simulation criterion, in order to achieve comparisons between free flight or CFD results to wind tunnel results, has to be determined.

The AGARD methodology (as cited in Haines [8]) proposes that CFD calculations should be computed prior to the wind tunnel measurements in order to determine the critical Reynolds number for a given simulation criterion. Suggestions for the simulation criterion could be;

- a zero-level criterion such as the boundary layer momentum thickness at the trailing edge of the equivalent flat plate, or
- a “first-order” criterion such as shock position, shock strength or the boundary layer momentum or displacement thickness at the trailing edge of the real wing, or
- a “second-order” or local criterion such as the boundary layer shape factor near the trailing edge of the non-dimensional length of a shock-induced separation bubble.

A typical appearance of the simulation criterion as a function of Reynolds number is shown in Figure 8. When the critical Reynolds number has been determined one could then scale the wind tunnel data as;

- follow the measured trend from  $Re_{test}$  to  $Re_{crit}$  (extrapolate to  $Re_{crit}$  if  $Re_{test} < Re_{crit}$ )

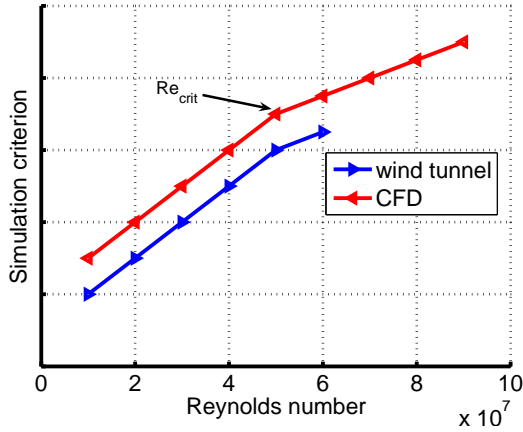


**Fig. 8** Simulation criterion as a function of Reynolds number showing a  $Re_{crit}$  at Reynolds number 50 million.

- move parallel to the computed trend for Reynolds numbers ranging from  $Re_{crit}$  to  $Re_{freeflight}$

A few different ways to perform the Reynolds number scaling is presented below.

#### 4.1 Reynolds number scaling using semi-empirical skin friction methods

A fairly frequent approach of scaling aerodynamic data with varying Reynolds number is the approach given by Wahls [17] amongst others. This approach implies that skin friction drag is estimated with equivalent flat plate theory, plus form factors, using the Blasius and Karman-Shoehnerr incompressible skin friction correlations for laminar and turbulent boundary layers respectively, with compressibility effects accounted for with the reference temperature method by Sommer and Short [15]. How the shape factors could be constructed is given by Covert [4] or Paterson [11] for example. Many companies do however have their own definitions of shape factors and scaling methodologies, and this is part of their competitive edge. [1] The extensive use of shape factors or other semi empirical methods which heavily relies on data from previously designed aircraft contradicts the idea that “understand the flow” is a better maxim than

“use the numbers from the last aircraft”, from Haines [8]. As a complement to shape factors based on previously designed aircraft and semi empirical methods is the usage of CFD methods. When CFD is used the skin friction and pressure drag is available for each component of the aircraft and an alternative way of constructing shape factors or drag due to camber etc is possible. The equation (1) has been modified from its original form in Paterson [11] where the free flight term on the right hand side has been replaced with CFD.

$$\frac{C_{D_p}}{C_{F_{WT}}} = \frac{C_{D_p}}{C_{F_{CFD}}} \quad (1)$$

When CFD calculations have been performed the ratio of drag due to pressure and skin friction is known. Using equation (1) gives the opportunity to scale the isolated skin friction of the corrected wind tunnel results to free flight Reynolds number.

The semi-empirical skin friction method used here is the Karman-Schoehnerr equation and compressibility effects are corrected with the Sommer-Short estimate using a recovery factor of 0.89. According to White[20], this value is in good agreement with experimental data for compressible turbulent flat plate flow. In figure 9, the Karman-Schoehnerr and Sommer-Short estimate has been anchored to the CFD data. The shift of the skin friction estimate was done by multiplication with a constant factor. The Reynolds number which the experimental data is anchored to, is typically the highest available Reynolds number data. The factor which anchors the skin friction estimate to the experimental data includes the effects of flow over curved surfaces and interference effects[4]. Using a constant factor to shift the skin friction estimate implies a constant influence of the effects due to flow over curved surfaces and interference effects for varying Reynolds number. Whether this is true or not needs to be determined. Here the data was anchored to the 38 million Reynolds number case in order to compare the extrapolated results with the computed CFD data at a higher Reynolds number.

If the drag of the wings, for example, are as-

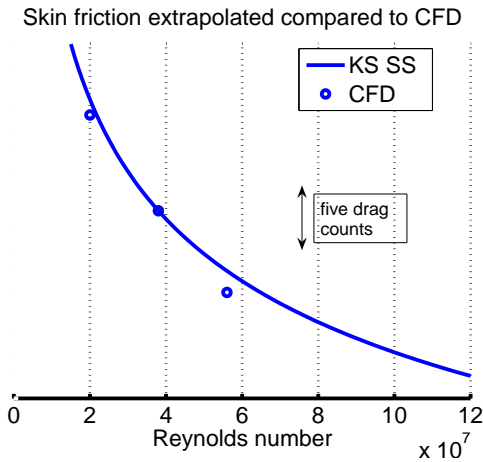


**Fig. 9** Skin friction estimated with Karman-Shoeherr and Sommer-Short methods anchored to CFD data at Reynolds number 38 million.

sumed to have the same proportion to the total drag for both wind tunnel and CFD results, skin friction could also be scaled part by part. The idea is that the extra information of using the characteristic length of each part will make the scaling more accurate. The shorter length scale of the vtp might not be the appropriate length scale for scaling the fuselage which is much longer. Equation (2) follows the idea of equation (1) and ratios between the corrected wind tunnel data is assumed to correlate to the CFD data. If this would not be true, some discrepancies in drag due to pressure or skin friction is present, or pseudo-Reynolds number effects has not been accounted for in the corrected wind tunnel data.

$$\frac{C_{D_{part}}}{C_{D_{aircraft\ WT}}} = \frac{C_{D_{part}}}{C_{D_{aircraft\ CFD}}} \quad (2)$$

If equation (2) holds the results from the CFD calculations could be used to determine each components drag due to skin friction. Each components skin friction could then be anchored to the highest available Reynolds number data and an appropriate method of extrapolating skin friction with Reynolds number could be used in order to estimate the free flight Reynolds number drag. In figure 10 the Karman-Shoeherr skin friction estimate with the Sommer-Short method has been used to scale each component of the air-

craft separately. The extrapolated drag of each component has been anchored to its drag predicted by the CFD calculation at Reynolds number 38 million.

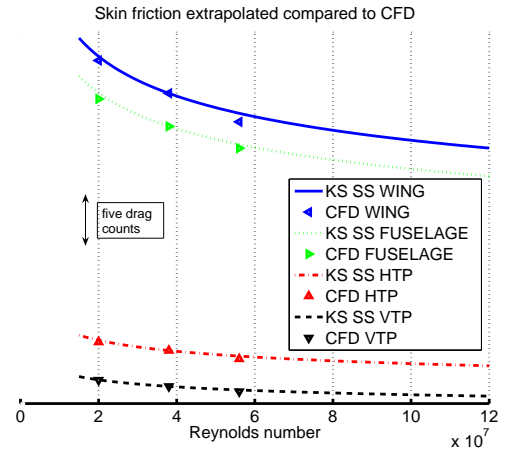


**Fig. 10** Skin friction estimated with Karman-Shoeherr and Sommer-Short methods for each part of the aircraft separately, anchored to CFD data at Reynolds number 38 million.

Combining the use of scaling the whole aircraft or each part separately and scaling skin friction or total drag with a semi empirical method results in four different results. These four results are shown in table 2 where the data is given as the extrapolated data minus the CFD data at Reynolds number 56 million in drag counts. The data has been rounded towards the closest integer.

**Table 2** Comparison of the extrapolated data and CFD in drag counts at Reynolds number 56 million.

	skin friction	total drag
part by part	2	-3
aircraft	2	-3

It is noticeable that scaling the aircraft skin friction part by part does not seem to imply an increased accuracy of the extrapolated results at Reynolds number 56 million compared to scaling the whole aircraft at once. The error in extrapo-

lating data is however lower when the skin friction is extrapolated compared to when the total drag is extrapolated.

The drag due to pressure varies with Reynolds number. Following the idea of Reichenbach [12], where an aerodynamic quantity is fitted to an interpolation curve, is utilized here for scaling drag due to pressure with varying Reynolds number. Reichenbach fits  $C_L$  to a function with Reynolds number as the variable and three constants. These three constants are then determined by three measurement points; one from CFD and two from wind tunnel tests. Here we fit drag due to pressure using the same type of function, see equation (3).

$$C_{dp} = C_1 + C_2(Re)^n \quad (3)$$

The three Reynolds numbers 20, 38 and 56 million for the CFD results were used to determine the constants. An extra calculation at Reynolds number 74 million were performed in order to evaluate the numerical fit of the CFD data. The results of the fitted data and CFD calculations are shown in figure 11.

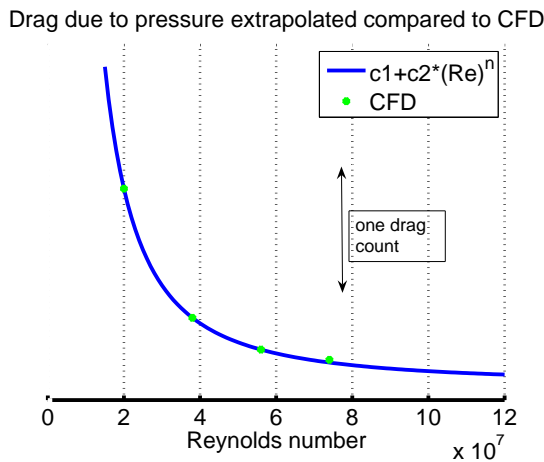


Fig. 11 Numerical fit of drag due to pressure.

The difference at the Reynolds number 74 million case between the numerically fitted data and the CFD calculation was approximately -0.02 drag counts. The root mean square (rms) of the errors for the numerical fit at the three lower Reynolds number compared to the CFD calcula-

tions was  $1.9 \times 10^{-9}$ . The condition number, see equation (4), of the problem was 0.05.

$$\text{condition number} = \max\left(\left|\frac{f'(x)}{f(x)}\right| \times |x|\right) \quad (4)$$

If equation (2) holds, equation (3) could be used to extrapolate wind tunnel drag due to pressure. The change in drag due to pressure for varying Reynolds number might give insight of when the critical Reynolds number has been reached and the only change in drag for an increase in Reynolds number is due to changes in skin friction. One alternative way of determining the critical Reynolds number could be when the drag due to pressure varies with one percent, comparing the critical and free stream Reynolds number conditions. This parameter is just a proposal and it might have to be corrected when other types of flow conditions are encountered. One proposed strategy of extrapolating Reynolds number data is;

- estimate from previous experience the critical Reynolds number.
- perform CFD calculations for at least three Reynolds numbers, some above and some below the estimated critical Reynolds number.
- calculate the drag due to pressure and fit the results to equation (3)
- determine the accuracy,  $\epsilon$ , which might be expected in the CFD and wind tunnel measurements.
- establish the critical Reynolds number as when the change in drag due to pressure is one percent of free flight conditions.
- examine trailing edge criterion behavior at the trailing edges of the wing, htp, vtp and fuselage in order to investigate additional local Reynolds number dependence (these local effects on drag might cancel each other when global drag is examined).

- determine  $Re_{crit} \pm \epsilon$  for both wind tunnel and CFD.
- investigate if there is any difference between critical Reynolds number from the CFD and wind tunnel measurements.
- visually inspect and determine whether there are any changes in the topological structure of the oil flow in both CFD and wind tunnel results or not. No large differences in oil flow topology should be visible when comparing Reynolds number data which are super critical.
- scale the wind tunnel data with CFD trends up to the critical Reynolds number and then further on to free flight conditions.

If no clear critical Reynolds number could be established this could be due to at least two factors; no clear critical Reynolds number exist for this specific type of flow, or the Reynolds number to which the extrapolation is done is below a critical Reynolds number. Regarding the last point of the proposed strategy, the Karman-Shoeherr and Sommer-Short methods have been used to evaluate the compressible skin friction variation and a numerical fit of the drag due to pressure in order to scale the data from Reynolds number 38 million to free flight conditions. The accuracy of the CFD method would not be a function of how much it would differ from the wind tunnel measurements, since this would regard the wind tunnel results to be the correct answer in an absolute sense. The accuracy in the CFD method would rather depend on the residual, mesh and turbulence modeling sensitivity. This would typically be known from experience in using a specific CFD code and turbulence model. It is not the absolute numbers that are important when determining the critical Reynolds number but the trends; the change, in some parameter, between the corrected wind tunnel data and CFD results (see figure 8) will hopefully be constant for varying Reynolds number. The accuracy in the wind tunnel would on the other hand depend on repeatability and accuracy in the measuring devices etc. The extra effort in investigating critical

Reynolds number, trailing edge criterion and oil flow topology will hopefully increase the understanding of the specific flow case at hand, revealing potential differences between CFD and wind tunnel measurements and improve scaling wind tunnel data to free flight conditions.

### 4.2 Inspection of local boundary layer properties for varying Reynolds number

When comparisons between either free flight, CFD or wind tunnel measurements and Reynolds number sensitivity are to be evaluated, some parameter of interest has to be chosen. When drag due to Reynolds number variation is the subject of the investigation, the local parameter  $c_f$ , seems to be a natural candidate for investigation. An accurate and robust (if it will be done at free flight conditions) way of measuring skin friction has to be determined. Measuring skin friction could be done in either a direct or an indirect manner. The direct measurement of skin friction could be done by using either small floating balances or through the use of surface-imaging interferometry. The former has the disadvantage of being susceptible to damage and thermal shifts and the latter is usually limited to laboratory settings. Preston tubes and boundary layer rakes are the two most common tools to indirectly estimate skin friction on vehicles. In the work by Whitmore [21] a combination of boundary layer rakes and Preston tubes are used to evaluate viscous forebody drag. A set of equations consisting of normalized boundary layer thickness, Reynolds number and Clauser parameter are used in order to estimate the local skin friction, momentum thickness, displacement thickness and boundary layer shape factor. These equations are solved in order to account for the entire viscous forebody drag including; effects of skin friction, forebody separation and forebody wakes and parasite drag due to protuberances. There exists a variety of empirical and semi-empirical methods to predict skin friction for flat plate flow. Methods such as those based upon the 1/7th power law and the logarithmic law relates  $c_f$  to  $Re_x$  and suffer from the difficulty of estimating the unknown origin, according to

Crook [5]. A variety of methods trying to compensate for the effect of an unknown transition position and pressure gradients are based on integrated boundary layer properties, like displacement and momentum thickness instead of the local Reynolds number. Two different methods of determining skin friction have been chosen in order to evaluate their accuracy in predicting trends of Reynolds number scale effects on local skin friction. One method from White [20], see equation (5), utilizes the local Reynolds number ( $Re_x$ ) and the correlation from Watson [19], see equation (6), utilizes Reynolds number based on local momentum thickness ( $Re_\theta$ ).

$$c_f = \frac{0.455}{\ln^2(0.06Re_x)} \quad (5)$$

$$c_f = 0.0097Re_\theta^{-0.144} \quad (6)$$

The evaluation of the two methods have been performed on the htp at positions corresponding to the dots in figure 12.

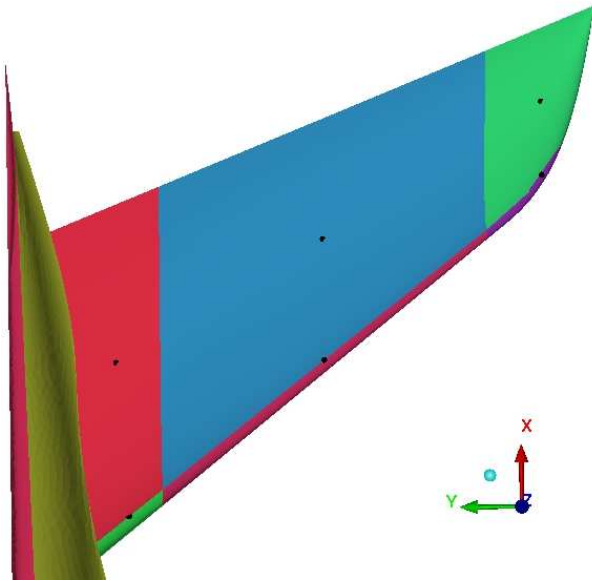


**Fig. 12** Htp seen from above, positions where skin friction were evaluated marked with dots.

The htp has been divided in twelve parts in total, three major parts: inboard, outboard and middle part which in turn has been divided into a front, an upper, a lower and a trailing edge

part. The major parts are approximately 25, 65 and 10% of the total wetted area of the htp, for the inboard, middle and outboard parts respectively. The measuring positions in chord-wise direction are located at 5 and 50% of the local chord length and at half of the trailing edge length in span wise direction for each major part respectively.  $Re_x$  and  $Re_\theta$  were evaluated at 20 and 38 million Reynolds number. The data were then linearly extrapolated to the 56 million Reynolds number case and compared to CFD calculations. Figure 13 shows the variation of  $Re_\theta$  as function of free stream Reynolds number and the extrapolated data for the middle top part of the htp. A

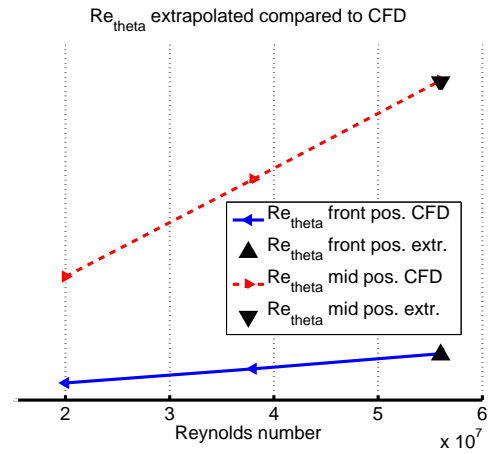


**Fig. 13**  $Re_\theta$  as function of  $Re_\infty$ , extrapolated and CFD results.

least square fit of the linear approximation of  $Re_\theta$  resulted in a rms of the error of 20 for the front position and 30 for the middle position. Note that the order of magnitude of  $Re_\theta$  is of  $10^4$ , so the fit of the linear extrapolation is judged as a very good approximation. The  $Re_\theta$  and  $Re_x$  from the 20 and 38 million cases using CFD calculations and the data extrapolated to 56 million Reynolds number were used to calculate  $c_f$ . The skin friction were then anchored to the 38 million Reynolds number CFD case in order to evaluate each methods capability to predict skin friction trends. A rms of the error for the twelve extrapolated results of skin friction compared to CFD were calculated. The method using equation (5) resulted in a rms of the errors of 0.95 drag counts

and the method using equation (6) resulted in a rms of the errors of 0.88 drag counts comparing extrapolated skin friction with CFD calculations at Reynolds number 56 million. Note that if any of these points shown in figure 13 would have been chosen as trailing edge criterion, neither of them would have revealed any major deviations with increasing Reynolds number which would have implied a critical Reynolds number (compare to the kink in figure 8 implying a typical flow topology change or a shock wave moving from an up or down stream position).

## 5 Conclusions

An aerodynamic assessment of a modern transonic transport aircraft has been evaluated with CFD methods at Reynolds number 20, 38 and 56 million with a free stream Mach number of 0.85 at an angle of attack of  $0^\circ$ . Reynolds number scaling of global drag and local skin friction has been evaluated. Scaling the aircraft skin friction with the Karman-Shoehnerr estimate and correcting compressible effects with the Sommer-Short method was accurate within 2 drag counts when comparing scaled results with CFD results at Reynolds number 56 million. Fitting the drag due to pressure at 20, 38 and 56 million Reynolds number and comparing the fitted data with CFD data at 74 million Reynolds number resulted in a deviation of approximately 0.02 drag counts. An investigation of scaling local skin friction was performed with two different methods in order to evaluate their capabilities of predicting changes in local skin friction due to a Reynolds number change. Marginal improvements were shown when skin friction were scaled with a method based on  $Re_\theta$  compared to a more classical estimate for turbulent flat plate flow. Both methods predicted variations in local skin friction fairly well.

## 6 Acknowledgements

Financial support to this work was provided by the REMFI project (contract AST3-CT-2004-502895), 6<sup>th</sup> EU framework programme. SNIC

and PDC are also acknowledged for their help and support with the parallel computer on which these calculations have been done.

## References

- [1] Barlow J. B, Rae W. H, and Pope A. *Low-Speed Wind Tunnel Testing*. 3 edition, Wiley-Interscience, 1999.
- [2] Bushnell D. M. Scaling: Wind tunnel to flight. *Annual Review of Fluid Mechanics*, Vol. 38, pp 111–128, 2006.
- [3] Casey M and Wintergerste T, editors. *Best Practice Guidelines*. Special Interest Group on "Quality and Trust in Industrial CFD", ERCOF-TAC, 2000.
- [4] Covert E. E. Thrust and drag: Its prediction and verification. *Progress in Astronautics and Aeronautics Series*, Vol. 98. AIAA, 1985.
- [5] Crook A. Skin-friction estimation at high reynolds numbers and reynolds-number effects for transport aircraft. *Annual Research Briefs*, pp 427–438. Center for Turbulence Research, 2002.
- [6] Eliasson P. Edge, a navier-stokes solver for unstructured grids. *Proc Proceedings To Finite Volumes for Complex Applications III*, pp 527–534, 2002.
- [7] European Commission, editor. *Aeronautics Research 2003-2006 projects*. Vol. Project synopses - volume 1 Research Projects from the first and second calls, Office for Official Publications of the European Communities, 2006.
- [8] Haines A. B. Scale effects on aircraft and weapon aerodynamics. *AGARD-AG-323*. AGARD, 1994.
- [9] Hellsten A. New advanced k-omega turbulence model for high-lift aerodynamics. *AIAA-2004-1120*, 2004.
- [10] Hemsch M. J and Morrison J. H. Statistical analysis of cfd solutions from 2nd drag prediction workshop. *Proc AIAAd-2004-0556*, 2004.
- [11] Paterson J, MacWilkinson D, and Blackerby W. A survey of drag prediction techniques applicable to subsonic and transonic aircraft design. *AGARD-CP-124*, pp 1–38, 1973.
- [12] Reichenbach S and McMasters J. A semiempirical interpolation technique for predicting full-

- scale flight characteristics. *AIAA-87-0427*, January 1987.
- [13] Saltzman E. J and Ayers T. G. Review of flight-to-wind-tunnel drag correlation. *Journal of Aircraft*, Vol. 19, No 10, pp 801–811, October 1982.
- [14] Schewe G. Reynolds-number effects in flow around more-or-less bluff bodies. *Journal of Wind Engineering and Industrial Aerodynamics*, Vol. 89, pp 1267–1289, 2001.
- [15] Sommer S. C and Short B. J. Free-flight measurements of turbulent-boundary-layer skin friction in the presence of severe aerodynamic heating at mach numbers from 2.8 to 7.0. *NACA-TN-3391*, March 1955.
- [16] Tysell L. An advancing front grid generation system for 3d unstructured grids. *ICAS-94-2.5.1*, 1994.
- [17] Wahls R, Owens L, and Rivers S. Reynolds number effects on a supersonic transport at transonic conditions. *AIAA*, 2001.
- [18] Wallin S and Johansson A. An explicit algebraic reynolds stress model for incompressible and compressible turbulent flows. *Journal of Fluid Mechanics*, Vol. 403, pp 89–132, 2000.
- [19] Watson R, Hall R, and Anders J. Review of skin friction measurements including recent high-reynolds number results from nasa langley ntf. *AIAA-2000-2392*, 2000.
- [20] White F. M. *Viscous Fluid Flow*. second edition, Mechanical Engineering, McGraw-Hill, 1991.
- [21] Whitmore S. A, Hurtado M, and Naughton J. W. A real-time method for estimating viscous forebody drag coefficients. Technical Report NASA/TM-2000-209015, NASA, January 2000.